



Evolutionary isolation of ryanodine receptor isoform 1 for muscle-based thermogenesis in mammals

Daniel P. Singh^{a,1} , Luke Pearce^{a,1} , Rocky H. Choi^a, Aldo Meizoso-Huesca^a, Stefan G. Wette^b , John W. Scott^{c,d}, Cedric R. Lambole^a, Robyn M. Murphy^b, and Bradley S. Launikonis^{a,2}

Edited by Susan L. Hamilton, Baylor College of Medicine, Houston, TX; received September 23, 2021; accepted December 5, 2022 by Editorial Board Member Andrew R. Marks

Resting skeletal muscle generates heat for endothermy in mammals but not amphibians, while both use the same Ca^{2+} -handling proteins and membrane structures to conduct excitation–contraction coupling apart from having different ryanodine receptor (RyR) isoforms for Ca^{2+} release. The sarcoplasmic reticulum (SR) generates heat following Adenosine triphosphate (ATP) hydrolysis at the Ca^{2+} pump, which is amplified by increasing RyR1 Ca^{2+} leak in mammals, subsequently increasing cytoplasmic $[\text{Ca}^{2+}]$ ($[\text{Ca}^{2+}]_{\text{cyto}}$). For thermogenesis to be functional, rising $[\text{Ca}^{2+}]_{\text{cyto}}$ must not interfere with cytoplasmic effectors of the sympathetic nervous system (SNS) that likely increase RyR1 Ca^{2+} leak; nor should it compromise the muscle remaining relaxed. To achieve this, Ca^{2+} -activated, regenerative Ca^{2+} release that is robust in lower vertebrates needs to be suppressed in mammals. However, it has not been clear whether: i) the RyR1 can be opened by local increases in $[\text{Ca}^{2+}]_{\text{cyto}}$; and ii) downstream effectors of the SNS increase RyR Ca^{2+} leak and subsequently, heat generation. By positioning amphibian and malignant hyperthermia-susceptible human-skinned muscle fibers perpendicularly, we induced abrupt rises in $[\text{Ca}^{2+}]_{\text{cyto}}$ under identical conditions optimized for activating regenerative Ca^{2+} release as Ca^{2+} waves passed through the junction of fibers. Only mammalian fibers showed resistance to rising $[\text{Ca}^{2+}]_{\text{cyto}}$, resulting in increased SR Ca^{2+} load and leak. Fiber heat output was increased by cyclic adenosine monophosphate (cAMP)-induced RyR1 phosphorylation at Ser2844 and Ca^{2+} leak, indicating likely SNS regulation of thermogenesis. Thermogenesis occurred despite the absence of SR Ca^{2+} pump regulator sarcolipin. Thus, evolutionary isolation of RyR1 provided increased dynamic range for thermogenesis with sensitivity to cAMP, supporting endothermy.

ryanodine receptor | skeletal muscle | thermogenesis | mammals | calcium

The transition from ectothermy to whole-body endothermy in some vertebrates (mammals and birds) has been a key to their evolutionary success. A major advantage in mammals is the ability to use relaxed muscles for thermogenesis to assist the maintenance of core body temperature. It has been shown that the generation of heat in resting skeletal muscle is significantly affected by ryanodine receptor (RyR) Ca^{2+} leak and the subsequent activity of the sarcoplasmic reticulum (SR) Ca^{2+} pump to maintain the steady level of SR $[\text{Ca}^{2+}]$ (1). Persistent RyR Ca^{2+} leak is a feature of healthy human muscle (2), constantly consuming ATP at the SR Ca^{2+} pump to maintain steady-state SR $[\text{Ca}^{2+}]$ ($[\text{Ca}^{2+}]_{\text{SR}}$) in the resting muscle. If the RyR Ca^{2+} leak rate can be regulated, then the resting muscle can generate more heat as it works harder to maintain steady state $[\text{Ca}^{2+}]_{\text{SR}}$ as a counter to a steepening temperature gradient across the surface of the body as the ambient temperature lowers. Such mechanisms have been suggested from indirect measurements (3, 4). In contrast, lower vertebrates do not generate heat from the SR of their resting muscles (1) and so use alternative means of cold tolerance (5, 6).

The separation of mammals from lower vertebrates in thermoregulatory capacity suggests a key component of muscle has altered during the evolution of mammals. A major difference may lay within the RyR isoforms present on the SR membrane. Amphibians and other lower vertebrates have two isoforms, α RyR and β RyR, whereas mammalian skeletal muscle has a single isoform, RyR1. In amphibians, the α RyR isoform is under the direct control of the dihydropyridine receptors (DHPR) and activated by voltage; and the β RyR isoform is sensitive to cytoplasmic Ca^{2+} , where increases in $[\text{Ca}^{2+}]_{\text{cyto}}$ cause regenerative release, known as Ca^{2+} -induced Ca^{2+} release (CICR) (7). In contrast, the RyR1 is coupled to the DHPR under the control of membrane voltage. Neither the α RyR nor RyR1 isoforms require any extracellular Ca^{2+} influx trigger during excitation–contraction (EC) coupling (8), suggesting that the role of CICR in skeletal muscle of amphibians, where it presents as a robust mechanism capable of depleting the SR, is one that does not involve the acute regulation of EC coupling. Complicating this matter is that the ability of CICR to directly open RyR1 remains controversial (9, 10). Some researchers suggest the RyR1 has sensitivity

Significance

A major evolutionary event in the rise of mammals was developing muscle-based thermogenesis. Mammals use muscle for heat generation while the muscle remains relaxed. The process of generating heat requires raising cytoplasmic $[\text{Ca}^{2+}]$ via RyR leak to hydrolyze ATP. We hypothesized that the transition to using muscle for heat generation required resistance to Ca^{2+} -activated regenerative Ca^{2+} release, a robust mechanism in lower vertebrates, and sensitivity to leak regulation by the sympathetic nervous system. We developed approaches that demonstrate resistance of RyR to opening by abrupt rises in $[\text{Ca}^{2+}]$, and heat generation via cAMP-activated RyR Ca^{2+} leak in mammals. We conclude the evolutionary loss of a Ca^{2+} -sensitive RyR isoform was important in RyR Ca^{2+} leak-based thermogenesis in mammals.

Author contributions: D.P.S., L.P., R.H.C., A.M.-H., and B.S.L. designed research; D.P.S., L.P., R.H.C., A.M.-H., S.G.W., and J.W.S. performed research; D.P.S., L.P., A.M.-H., S.G.W., J.W.S., C.R.L., R.M.M., and B.S.L. analyzed data; and D.P.S. and B.S.L. wrote the paper.

The authors declare no competing interest.

This article is a PNAS Direct Submission. S.L.H. is a guest editor invited by the Editorial Board.

Copyright © 2023 the Author(s). Published by PNAS. This article is distributed under Creative Commons Attribution-NonCommercial-NoDerivatives License 4.0 (CC BY-NC-ND).

¹D.P.S. and L.P. contributed equally to this work.

²To whom correspondence may be addressed. Email: b.launikonis@uq.edu.au.

This article contains supporting information online at <https://www.pnas.org/lookup/suppl/doi:10.1073/pnas.2117503120/-DCSupplemental>.

Published January 17, 2023.

to CICR (11–13), whereas others have presented evidence to the contrary (14–18). These differences in opinion may be linked to technical difficulties of examining CICR in muscle fibers.

Interestingly, the RyR Ca^{2+} leak rate in the resting muscle of amphibians and mammals is 2 to 3 $\mu\text{M}/\text{s}$ and 14 to 30 $\mu\text{M}/\text{s}$, respectively (19–21). The magnitude difference in SR Ca^{2+} leak suggests a pivotal physiological role for leak that separates amphibians and mammals. The local $[\text{Ca}^{2+}]$ at the cytoplasmic face of the RyR must be higher in mammals than toad, due to the RyR leak (2, 22). The high local $[\text{Ca}^{2+}]$ at the cytoplasmic side of the RyR must be able to increase further without opening the RyR1s; otherwise, the result would be uncontrolled Ca^{2+} release. We expect resistance of RyR1 to opening by cytosolic $[\text{Ca}^{2+}]$ to be a fundamental property of this channel, where leak is an effective modulator of thermogenesis in resting muscle (1). Secondly, we hypothesized that the presence of a robust CICR mechanism in amphibian muscle may be key in limiting SR Ca^{2+} load (23) and therefore RyR Ca^{2+} leak rate; a means of restricting ATP use at the SR Ca^{2+} pump (22). This is consistent with the demonstration that the SR Ca^{2+} pump of resting fibers from toad has a reduced load compared to resting fibers from mouse (1). In addition to this second point, CICR remains essential to EC coupling in the heart where it activates opening of the RyR2 isoform due to Ca^{2+} influx through the L-type Ca^{2+} channel inducing CICR (24). The loss of the need for Ca^{2+} influx to open amphibian RyR during EC coupling but retention of CICR in the muscle is consistent with a contrasting role for the mechanism in amphibian skeletal muscle compared to heart.

We suspected that the isolation of RyR1 in mammalian skeletal muscle may have been a key evolutionary step that provided tolerance to increased RyR Ca^{2+} leak to provide thermogenic potential, where Ca^{2+} leak increases the local $[\text{Ca}^{2+}]_{\text{cyto}}$ at the SR Ca^{2+} pump, to increase the rate of ATP hydrolysis, heat generation, and basal metabolism. The absence of CICR in RyR1 would allow for the resting state of the muscle to be maintained, as Ca^{2+} release from a heavily Ca^{2+} -loaded SR is avoided. In parallel, these arguments allow us to propose that the presence of a RyR isoform in skeletal muscle supporting CICR may be a key defining factor in the ectothermic lifestyle of lower vertebrates (restricting energy use in the resting animal). However, the properties of RyRs in response to rising cytosolic Ca^{2+} in resting and unstimulated (by voltage) muscle remain controversial because it has not been simple to address how the RyR of unstimulated muscle responds to an abrupt rise in local $[\text{Ca}^{2+}]$. To do this, we generated Ca^{2+} waves in toad, human, or mouse mechanically skinned skeletal muscle fibers that were positioned perpendicularly to each other, so that their intersection provided a local area that could receive an abrupt rise in $[\text{Ca}^{2+}]$, from which the properties required to initiate a Ca^{2+} wave in the quiescent fiber could be observed under identical ionic conditions. By inducing Ca^{2+} waves under an exogenous agonist in muscle fibers from Queensland cane toads (*Rhinella marina*), human muscle susceptible to malignant hyperthermia and *RYR1* knock-in (KI) mouse fibers (25), we skewed the conditions to that most likely to observe Ca^{2+} waves initiated by CICR (15). We found that the isolated RyR1 of mammalian skeletal muscle continued to provide resistance to activation by cytosolic $[\text{Ca}^{2+}]$ even under these extreme conditions, allowing SR Ca^{2+} load to increase, providing driving force for increased RyR Ca^{2+} leak that is a platform for thermogenesis in relaxed muscle (1). Further, we show that brief treatment with cyclic adenosine monophosphate (cAMP) causes RyR1 phosphorylation, to increase Ca^{2+} leak and $[\text{Ca}^{2+}]$ at the SR Ca^{2+} pump and thus increase ATP hydrolysis and heat generation, consistent with regulation by the sympathetic nervous system (SNS). This increase in heat generation occurred in the absence of sarcolipin.

Results

In the following section, we image the movements of Ca^{2+} in the cytoplasm and SR as local $[\text{Ca}^{2+}]_{\text{cyto}}$ is abruptly increased in a quiescent fiber to activate Ca^{2+} release through the RyR with a technique that avoids movement or agitation artefacts and photodamage that are often induced in other methods used to raise local $[\text{Ca}^{2+}]_{\text{cyto}}$. We use mechanically skinned fibers, where the outer sarcolemma is peeled away, providing direct access to the cytoplasmic environment and experimental manipulation of its ionic composition (26). Our approach allows amphibian and mammalian muscle fiber properties to be compared simultaneously under identical ionic conditions. We use toads which are well-known to display robust CICR (27); and malignant hyperthermia-susceptible (MHS) fibers with gain-of-function *RYR1* mutations with RyRs that display leak and high susceptibility to opening by exogenous agonists (2, 22, 25). We provide a separation of the RyR Ca^{2+} handling properties of the respective fibers, which is required to assess their suitability to maintaining thermogenesis in the resting muscle.

Increased Local Cytosolic Ca^{2+} Causes Wave Activation. Fig. 1 shows a series of experiments where skinned fibers from toad, human MHS, or control human malignant hyperthermia non-susceptible (MHN) skeletal muscle were positioned perpendicular to each other (crossed-over) so that the fibers were in contact at a common intersection. This approach was termed “dual species” cross fiber preparations. The addition of 1 mM halothane to the cytosolic bathing solution of skinned fibers induced Ca^{2+} wave generation in toad and human MHS-skinned fibers. Critically, a Ca^{2+} wave travelling along one fiber abruptly imposes a high concentration of Ca^{2+} at the intersection with the quiescent fiber.

Fig. 1A and Movie S1 show a Ca^{2+} wave passing along the MHS fiber. When the wave transected the junction with the toad fiber, Ca^{2+} waves were generated immediately along the toad fiber in both directions. In the converse situation, a Ca^{2+} wave propagating along the toad fiber required a delay of ~3 s at the junction before Ca^{2+} waves were initiated in both directions on the mammalian fiber (Fig. 1B and Movie S2). In contrast, Ca^{2+} waves travelling along a toad fiber continuously failed to activate Ca^{2+} waves on a quiescent human MHN fiber as it passed through the junction of the fibers (Fig. 1C and Movie S3).

We also performed cross experiments where the fibers were both from toad or both from human MHS muscle (termed “single species” preparations) and were subjected to halothane to generate Ca^{2+} waves (SI Appendix, Fig. S1). The results of the single and dual species experiments are summarized in Fig. 1D, showing the average amount of time the Ca^{2+} wave from the “active” fiber spent at the junction prior to the activation of Ca^{2+} waves in the “quiescent” fiber. In human MHS and toad muscle fibers, there was a mean of 3.07 ± 0.16 s and 0.46 ± 0.02 s delay at the fiber junction prior to the quiescent fiber Ca^{2+} wave activation, respectively ($P < 0.0001$). When analyzed separately, we found no difference in this parameter in single or dual species experiments (Fig. 1E) which indicated that a significant difference in Ca^{2+} flux amplitude, as seen between human MHS fibers (2.06 ± 0.07 F/F₀) and toad fibers (2.48 ± 0.07 F/F₀, $P = 0.004$) (Fig. 1F), did not affect the initiation of Ca^{2+} waves in quiescent fibers. That is, in toad fibers, a smaller amplitude Ca^{2+} wave (arriving from human MHS fibers) still caused an immediate activation of Ca^{2+} release. In human MHS fibers, a larger amplitude Ca^{2+} wave (arriving from toad fibers) was unable to promote a CICR mechanism, demonstrating cytosolic Ca^{2+} resistance.

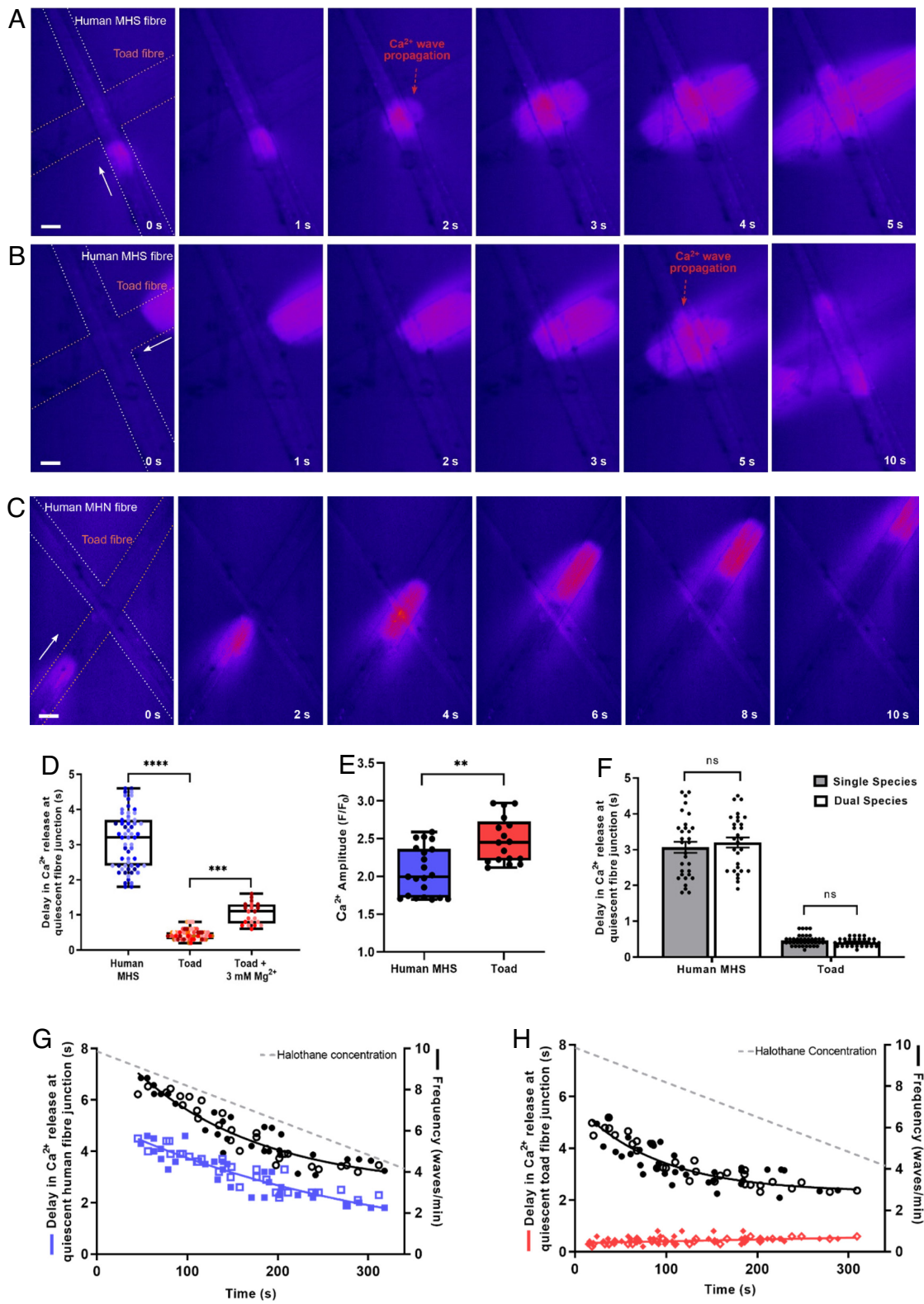


Fig. 1. Sensitivity of RyR isoforms to abruptly raised cytoplasmic Ca²⁺. Selected cytoplasmic rhod-2 fluorescence images of toad fibers “crossed-over” human MHS and MHN fibers during Ca²⁺ wave propagation in the presence of halothane. Dotted lines outline the fibers. *A*, a Ca²⁺ wave propagation along the MHS fiber (“activator fiber”) reaches the fiber intersection where Ca²⁺ waves are quickly activated in the quiescent toad fiber in both directions. *B*, a Ca²⁺ wave on the toad activator fiber reaches the intersection with the MHS fiber and takes several seconds to activate Ca²⁺ waves in the quiescent fiber. Note, both *A* and *B* are from the same preparation. *C*, the Ca²⁺ wave along the activator toad fiber passes the junction with the MHN fiber without initiating any waves in the quiescent fiber. *D*, the time a Ca²⁺ wave from the activator fiber spent at the junction with the quiescent fiber before waves were initiated in the quiescent fiber. Comparison of MHS (N = 5 individuals, n = 18 preparations), toad (N = 10 toads, n = 26 preparations), and toad muscle exposed to 3 mM Mg²⁺ (N = 4 toads, n = 8 preparations) (nested one-way ANOVA with Tukey's post hoc). Data points obtained from different individuals and organisms are indicated by different shades of blue and red, respectively. *E*, the Ca²⁺ wave amplitudes in toad and human fibers (nested t test). *F*, delay in Ca²⁺ wave activation results presented for crosses of “same species” (toad × toad; and human × human) and “dual species” (toad × human). *G* and *H*, time to propagate Ca²⁺ waves in quiescent fiber and Ca²⁺ wave frequency in activator fiber MHS and toad fibers, respectively, is plotted against time in halothane. The decline in [halothane] in solution is plotted on the graphs. Solid data points represent data obtained from single species preparations. Open data points represent data obtained from dual species preparations. Data presented in *D*, *E*, and *F* as box and whisker plots (median, box indicates 25% and 75% percentile, whiskers indicate min and max data points). **P < 0.01, ***P < 0.001, ****P < 0.0001, ns = not significant. (Scale bar, 50 μm.)

To confirm that toad fibers displayed a short activation time due to robust CICR, we performed the same cross experiments (toad fibers only) in the presence of 3 mM Mg²⁺ because Mg²⁺ decreases CICR activity by acting as a competitive antagonist to Ca²⁺ binding at the Ca²⁺ activation site of the RyR and also as an agonist of Ca²⁺ at the Ca²⁺ inactivation site (28). Consequently, a significant difference in delay of Ca²⁺ wave activation was observed in toad muscle when Mg²⁺ was increased from 1 mM to 3 mM (1.04 ± 0.07 s, $P = 0.0007$) (Fig. 1D).

In these experiments, halothane was added to the solution bathing the fiber in an open experimental chamber. Once exposed to air, halothane immediately begins to evaporate from solution. We calculated an evaporation rate of $0.16\% \text{ s}^{-1}$ (SI Appendix, Fig. S2). The decline in [halothane] over time provided an opportunity to examine the effect of cytoplasmic [agonist] on Ca²⁺ wave frequency rate and Ca²⁺ wave activation rate. This was important because the result would provide an indication of how sensitive the RyR was to cytoplasmic agonists in the presence of high [Ca²⁺]_{cyt}. Declining [halothane] was consistent with a decrease in Ca²⁺ wave frequency in the “activator” fibers from both human and toad muscle (Fig. 1 G and H). This is consistent with the RyRs progressively recovering their stability as halothane evaporated from the bathing solution of the fibers, making it harder for Ca²⁺ waves to be initiated. Concurrently with the decrease in Ca²⁺ wave frequency, quiescent human MHS fibers displayed a shortened delay in Ca²⁺ wave activation from 4.6 s to 1.8 s across the 5-min period of exposure to declining [halothane] (Fig. 1G). In contrast, toad quiescent fibers consistently activated Ca²⁺ waves within approximately 0.5 s in response to abrupt rises in [Ca²⁺]_{cyt} delivered from the activator fibers regardless of [halothane] (Fig. 1H). The results of Fig. 1 indicate that toad fibers are highly sensitive to [Ca²⁺]_{cyt}, even at low [agonist]. The sensitivity to [Ca²⁺]_{cyt} is consistent with a robust CICR at the cytoplasmic side of the RyR, presumably βRyR (29–31). In contrast, the delayed activation of Ca²⁺ waves in the quiescent fibers from human MHS muscle suggests this is not the case for RyR1.

The experiments presented in Fig. 1 were performed at room temperature (22 ± 1 °C). The temperature of the muscles in the body will be much higher than this, so we checked that the RyR properties were not changed by the low ambient temperature in which the experiments presented in Fig. 1 were performed at. To do this, we performed similar experiments on a confocal microscope with the stage enclosed by a temperature-controlled incubation chamber, which allowed us to set the temperature at 32 ± 1 °C. Cross experiments were performed under these conditions in toad and heterozygous *RYR1* KI mouse muscle fibers after a ~10-min equilibration period in the incubation chamber. Halothane was again used as the stimulus for eliciting Ca²⁺ waves. Under these conditions, the delay at quiescent fibers to generate Ca²⁺ waves following the abrupt rise in the local [Ca²⁺]_{cyt} due to the passing Ca²⁺ wave along the active fiber was 1.79 ± 0.09 s in mouse fibers and 0.53 ± 0.06 s in toad fibers ($P < 0.0001$) (SI Appendix, Fig. S3). There was also a significant decrease in delay of Ca²⁺ wave activation within mouse fibers when at 32 °C compared to room temperature ($P < 0.0001$) but no significant difference in toad fibers ($P = 0.6055$) (SI Appendix, Fig S3). The maintained difference in delay time between amphibian and mammalian muscle for Ca²⁺ wave activation (at both 32 °C and 22 °C) indicates that the mechanisms activating Ca²⁺ release through the RyR are not altered by temperature. Therefore, we can reasonably expect that these RyR properties represent those occurring in the body.

RyR1 is Sensitive to Non-Ca²⁺ Cytoplasmic Agonists and [Ca²⁺]_{SR}. The delay in activation of a Ca²⁺ wave in quiescent human fibers may be the time required for the SR to load Ca²⁺, so that a

[Ca²⁺]_{SR} threshold for RyR opening can be reached. This would be consistent with the decreased activation time of the waves as bathing solution [halothane] and Ca²⁺ wave frequency in mammalian fibers decreased with time (Fig. 1G) because the RyRs became more stable allowing [Ca²⁺]_{SR} to increase prior to the arrival of the abrupt increase in [Ca²⁺]_{cyt}. To test this, we performed further cross fiber experiments but where one of the fibers was loaded with fluo-5N into the SR to unambiguously monitor [Ca²⁺]_{SR} in the quiescent fiber as a Ca²⁺ wave met the junction of the two fibers. Fig. 2A shows an example of crossed fiber experiments (split channel images can be seen in SI Appendix, Fig. S4) using skinned fibers from mice heterozygous for a gain-of-function *RYR1* mutation (20). The fibers are crossed at a 45° angle. A Ca²⁺ wave enters from the top left of the image and as it approaches the junction of the two fibers, [Ca²⁺]_{SR} begins to increase at the left in the quiescent fiber due to the raised [Ca²⁺]_{cyt} in this region. A 3D plot in Fig. 2B shows the evolution of [Ca²⁺]_{SR} in the quiescent fiber, where [Ca²⁺] increases during the time that the Ca²⁺ wave enters and passes through the junction. Fig. 2C shows the spatiotemporal profile at the junction between fibers. The Ca²⁺ wave arriving from the activator fiber is represented by the purple line and the SR Ca²⁺-dependent fluo-5N fluorescence from the quiescent fiber is represented in green. There are four examples of activator Ca²⁺ waves reaching the junction of the fibers. In the first, second, and fourth Ca²⁺ waves, the Ca²⁺ wave reaching the junction caused a rise in [Ca²⁺]_{SR} that preceded the activation of the Ca²⁺ wave in the quiescent fiber. The rise in [Ca²⁺]_{SR} occurred for 2 to 3 s until there was activation of the subsequent Ca²⁺ waves. In the third activator Ca²⁺ wave, its lower amplitude induced only a small increase in [Ca²⁺]_{SR} compared to the other cases. No Ca²⁺ wave activation occurred in the quiescent fiber. Collectively, these data show that the activation of the Ca²⁺ wave in the quiescent fiber requires [Ca²⁺]_{SR} to increase to a threshold to open the RyR in the presence of agonist.

We performed similar experiments with crossed-over toad-skinned fibers, where one fiber had fluo-5N loaded into the SR (Fig. 2 D–F). Fig. 2F shows two examples of activator Ca²⁺ waves reaching the junction of the quiescent fiber. In each case, the activation of the Ca²⁺ wave in the quiescent fiber occurred with an immediate depletion of [Ca²⁺]_{SR}. No preceding rise in [Ca²⁺]_{SR} was needed to cause the quiescent toad fiber to generate a Ca²⁺ wave. Fig. 2D shows merged brightfield, rhod-2 and fluo-5N confocal images during this event. The 3D histogram in Fig. 2E shows the rapid decrease in [Ca²⁺]_{SR} in the quiescent fiber as wave propagation occurred.

Since we expected that the resistance to [Ca²⁺]_{cyt} in the mammalian fibers may allow the activation of the RyR1 to be a function of [agonist] and [Ca²⁺]_{SR}, we used a single fiber approach to better resolve the Ca²⁺ wave activation with the [Ca²⁺]_{SR} during the decline of [halothane]. To do this, we monitored [Ca²⁺]_{SR} with fluo-5N and cytoplasmic Ca²⁺ with rhod-2 during application of agonist to a single human MHS-skinned fiber (Fig. 3A). Fig. 3 shows cytoplasmic and SR Ca²⁺-dependent fluorescence signals from single MHS-skinned fibers in the presence of either halothane or caffeine. In these experiments, the use of halothane and caffeine provided [agonist] that declined and remained constant, respectively. In both cases, the application of agonist causes an immediate release of Ca²⁺ from the SR and a partial depletion of [Ca²⁺]_{SR}. As the cytoplasmic Ca²⁺ is resequestered by the SR concomitantly with the decline of the cytoplasmic Ca²⁺ transient, there is a rise of [Ca²⁺]_{SR}. In the examples for both halothane and caffeine, the [Ca²⁺]_{SR} reaches a value of approximately 0.35 mM, triggering another release of Ca²⁺. This [Ca²⁺]_{SR} threshold for Ca²⁺

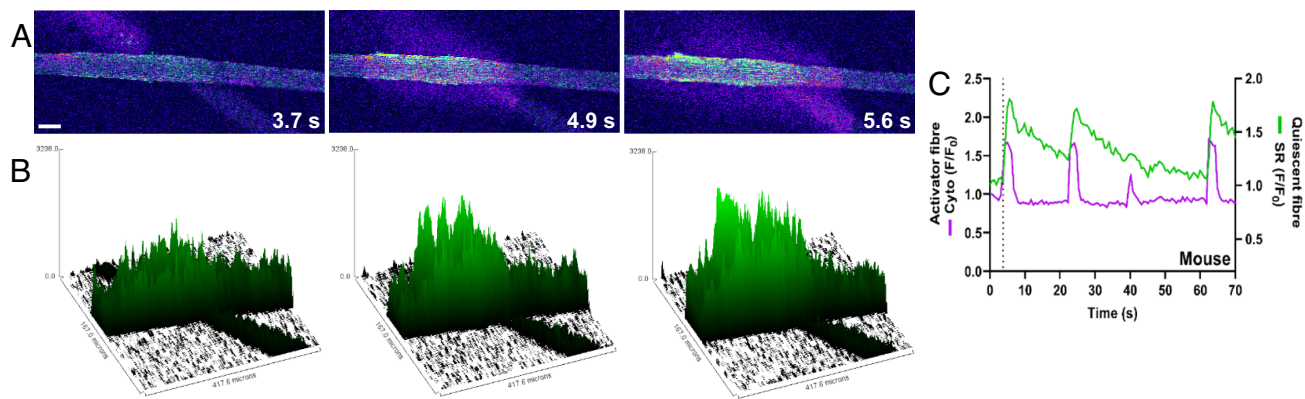
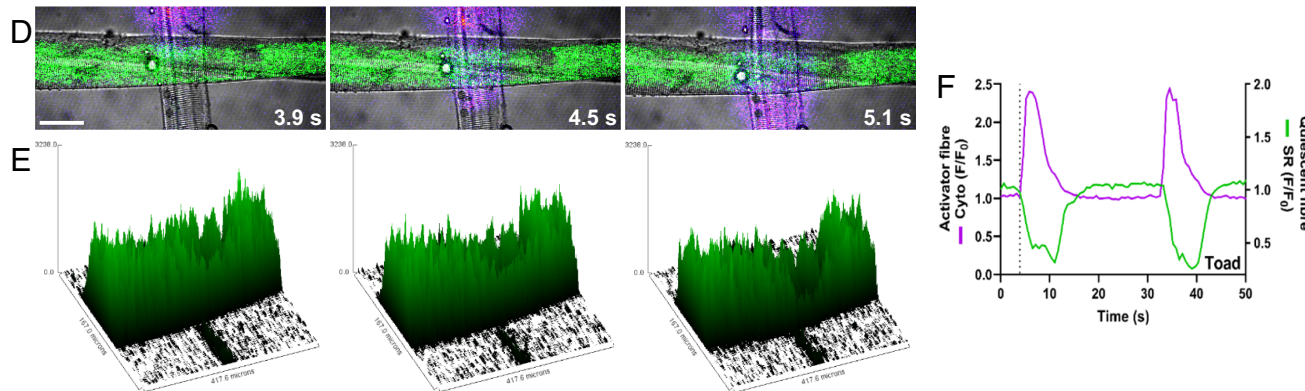
Mouse**Toad**

Fig. 2. Luminal activation of Ca^{2+} wave propagation in mammalian fibers. Two crossed-over fibers were placed in physiological solution containing rhod-2. One fiber contained SR fluo-5N A, representative merged cytoplasmic rhod-2 and SR fluo-5N fluorescence images of a RyR1 KI mouse shows Ca^{2+} uptake into the SR of the quiescent fiber once a Ca^{2+} wave from the active fiber reaches the junction. B, 3D fluo-5N fluorescence plot of adjacent frame in A shows the localized increase of Ca^{2+} in the quiescent fiber. C, spatially-averaged profiles of rhod-2 and fluo-5N fluorescence from the fiber junction in A. Note the low-amplitude cytoplasmic wave at 40 s fails to load the quiescent fiber to threshold level for wave activation in the quiescent fiber. D, merged cytoplasmic rhod-2, SR fluo-5N fluorescence, and transmitted light images in toad fibers show a time lapse of a wave from the active fiber passing the junction and instantly activating the quiescent fiber, indicative of CICR. E, 3D fluo-5N fluorescence plot of adjacent image in D. Note the immediate decrease in SR Ca^{2+} once the wave meets the junction and activates the quiescent fiber. F, rhod-2 and fluo-5N profiles of the images in D. (Scale bar, 50 μm .) Similar results were obtained on all 8 mouse and all 8 toad preparations.

release under the initial application of caffeine or halothane is significantly below the endogenous resting level of the $[\text{Ca}^{2+}]_{\text{SR}}$ of 0.5 to 0.58 mM in the absence of agonist. There continues to be repeated releases of Ca^{2+} as $[\text{Ca}^{2+}]_{\text{SR}}$ reaches about 0.35 mM following the resequestering of released Ca^{2+} .

As seen in Fig. 1, $[\text{halothane}]$ and wave frequency decreased in parallel. In conjunction with the decrease in wave frequency, the $[\text{Ca}^{2+}]_{\text{SR}}$ threshold for activation of Ca^{2+} release increased (Fig. 3B). In the presence of 3 mM caffeine (which is nonvolatile), a persistent Ca^{2+} wave frequency and $[\text{Ca}^{2+}]_{\text{SR}}$ threshold for Ca^{2+} release activation was observed (Fig. 3C). A summary of $[\text{Ca}^{2+}]_{\text{SR}}$ threshold for Ca^{2+} release in the presence of halothane and caffeine over time is shown in Fig. 3D. Together, these results indicate that the opening of the RyR in human muscle is a function of the RyR [agonist] and $[\text{Ca}^{2+}]_{\text{SR}}$.

cAMP and Heat Generation. The means in which mammalian skeletal muscle may increase thermogenesis physiologically via an endogenous agonist is unclear because of inherent problems in detecting changes in muscle fiber subcellular function in a preparation with an intact SNS that is sensitive to changes in ambient temperature. However, cold exposure in mammals has been shown to increase skeletal muscle non-shivering thermogenesis (4), which strongly suggests that the SNS must direct the need

for upregulating thermogenic processes at the muscle. Consistent with this, low ambient temperatures trigger the SNS to release catecholamines, which then have several downstream effects, including the activation of cAMP and eventual phosphorylation of the RyR1 (32–34). As such, we suspected that cAMP would phosphorylate RyR to increase RyR leak.

Initially, cAMP was applied to WT and *RYR1* KI mice, at concentrations of 100 μM , 200 μM , 500 μM , and 1 mM, to assess genotype-specific effects. cAMP generated Ca^{2+} waves in both groups, though there was no marked change in amplitude (F/F_0) of Ca^{2+} release as concentrations were increased (Fig. 4A). Most prominently, however, was the increasing wave frequency with increasing concentrations of cAMP in both the WT and *RYR1* KI fibers (Fig. 4B). Like the exogenous agonists, cAMP had a greater effect on *RYR1* KI compared to WT fibers, likely due to the reduced stability of the RyR1 closed state in the mutant fibers. Critically, a difference in response to 100 μM cAMP was found between the WT and *RYR1* KI fibers, where WT failed to respond with Ca^{2+} waves at this concentration. At 100 μM cAMP, we expected that cAMP may induce Ca^{2+} leak from the RyR1 in WT skeletal muscle, which would be important step in the SNS regulating non-shivering thermogenesis. To determine this, we employed an assay which uses the Ca^{2+} -sensitive dye rhod-5N trapped in the sealed t-system of skinned fibers to detect the rate

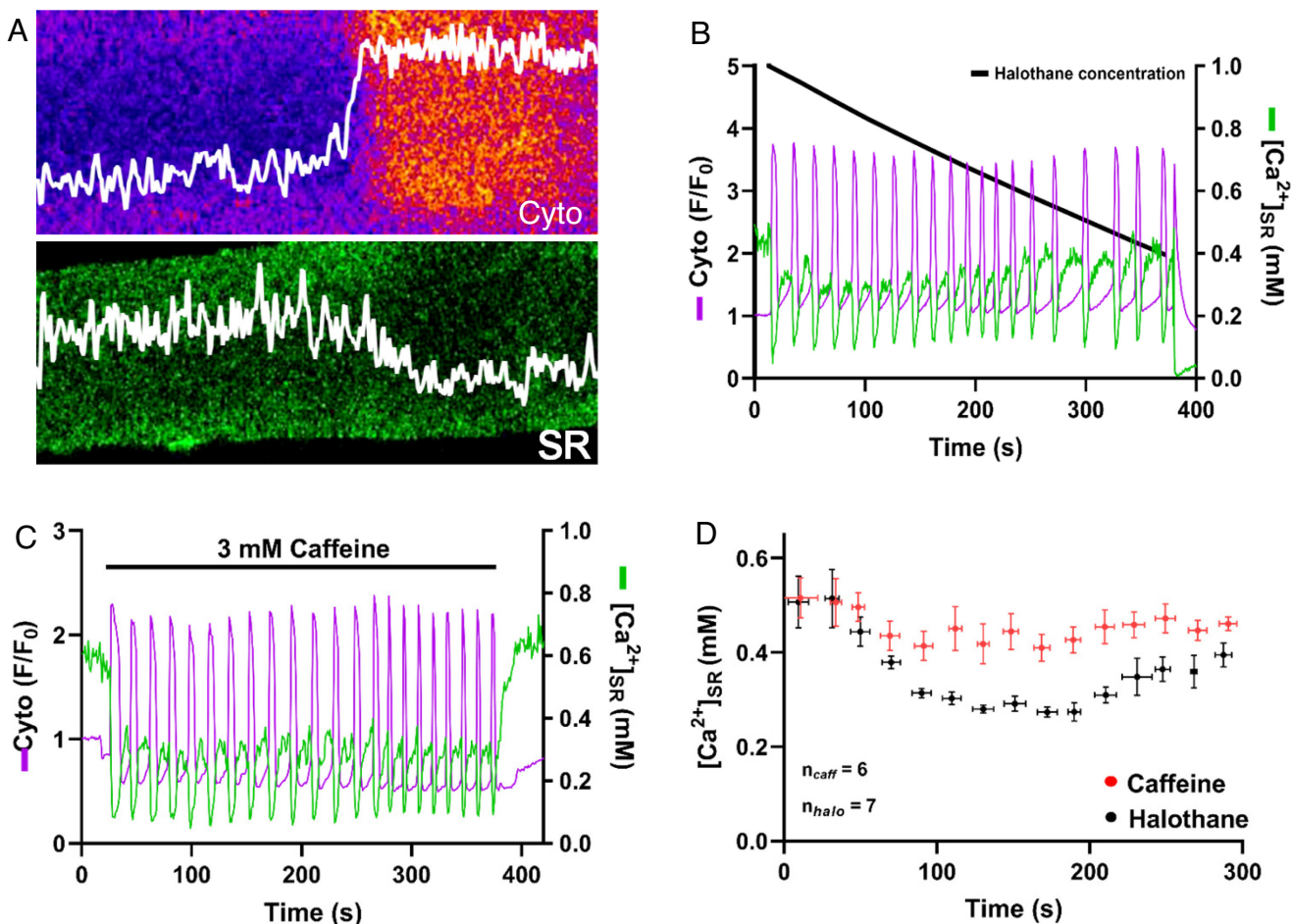


Fig. 3. The activation of Ca^{2+} waves in human MHS muscle by $[\text{Ca}^{2+}]_{\text{SR}}$ and [agonist]. *A*, cytoplasmic rhod-2 (*Top*) and SR fluo-5N fluorescence (*Bottom*) images in a human muscle fiber. The spatially averaged line fluorescence is superimposed in white on images. *B, C*, cytoplasmic rhod-2 and $[\text{Ca}^{2+}]_{\text{SR}}$ transients during the application of halothane and caffeine, respectively, in a skinned fiber from human MHS muscle. A large release of Ca^{2+} is immediately activated by the application of agonist and Ca^{2+} waves follow in both *B* and *C*. Each Ca^{2+} wave after the initiate release is activated as the $[\text{Ca}^{2+}]_{\text{SR}}$ reaches a certain threshold. In *B*, the $[\text{Ca}^{2+}]_{\text{SR}}$ threshold begins to increase as [halothane] decreases. In *C*, the $[\text{Ca}^{2+}]_{\text{SR}}$ threshold for Ca^{2+} wave activation remains generally steady as the [agonist] remains steady. *D*, summary of $[\text{Ca}^{2+}]_{\text{SR}}$ threshold for Ca^{2+} wave activation against time in each agonist. Note that an initial equilibration period of ~100 s passed across in the average of all fibers before the low $[\text{Ca}^{2+}]_{\text{SR}}$ was met. Data in *D* are presented as mean \pm SEM, $n = 6$ to 7.

that Ca^{2+} is translocated from the junctional space into the t-system after it is leaked from the RyR1 (2).

Fig. 4*C* shows a representative spatially averaged trace of the t-system rhod-5N fluorescence transient during successive exposures to cytoplasmic solutions that affect Ca^{2+} -handling. Initially in the presence of caffeine, $[\text{Ca}^{2+}]_{\text{t-sys}}$ was low due to the activation of store-operated Ca^{2+} entry (SOCE) as the SR is depleted (36). The wash-out of caffeine and substitution with standard loading solution with 100 nM $[\text{Ca}^{2+}]_{\text{cyto}}$ allows the SR to refill with Ca^{2+} , simultaneously allowing the $[\text{Ca}^{2+}]_{\text{t-sys}}$ to rise to millimolar levels. The application of 100 μM cAMP to the fiber after it has equilibrated with the standard solution resulted in a further increase in the $[\text{Ca}^{2+}]_{\text{t-sys}}$. This is indicative of the RyR1 leaking more Ca^{2+} to the junctional space, activating PMCA to move Ca^{2+} into the t-system (2). To check the change in $[\text{Ca}^{2+}]_{\text{t-sys}}$ was due to increased RyR1 activity, the RyR1 was blocked with 1 mM tetracaine (2). This manoeuvre caused $[\text{Ca}^{2+}]_{\text{t-sys}}$ to decrease below the level observed in the control solution.

During adrenergic stimulation and cAMP release, PKA phosphorylates several skeletal muscle targets in addition to the RyR (33). By applying a combination of tetracaine and cAMP together, it was possible to observe non-RyR effectors on the $[\text{Ca}^{2+}]_{\text{t-sys}}$ assay. The application of both tetracaine and cAMP together showed no significant difference compared to tetracaine alone ($P > 0.05$). This

suggested that cAMP directly affects the RyR1. Together, 100 μM cAMP did not activate Ca^{2+} release in WT mouse skeletal muscle; however, it did induce an increase in RyR Ca^{2+} leak (Fig. 4*D*).

In the above experiment, it was possible that cAMP increased leak via activation of the SR Ca^{2+} pump, to increase $[\text{Ca}^{2+}]_{\text{SR}}$ or by directly decreasing the stability of the RyR1 itself, to cause increased Ca^{2+} leak. Additionally, the increased leak under cAMP should increase the heat generated by the SR. To examine both issues, we used the temperature-sensitive dye ER thermo-yellow (ERTY) to measure the temperature of the SR under the application of cAMP (1). This experiment effectively monitors the activity of the SR Ca^{2+} pump, which is setting the SR temperature. The advantage is that the contribution of the RyR1 Ca^{2+} leak to SR Ca^{2+} pump heat generation; and heat generation from the isolated SR Ca^{2+} pump due to Ca^{2+} slippage through the pump (37, 38) can be examined in a single fiber preparation.

Fig. 4*E* shows images of a mechanically skinned fiber from WT mouse where fluo-5N and ryanodine were applied to a subsection of the preparation (upper image) and ERTY was evenly loaded to the entire fiber (lower image). The introduction of ryanodine causes a local inhibition of RyR1s in the region stained by fluo-5N (green signal in Fig. 4*E*), while the rest of the preparation maintains functional RyR1s. By introducing cAMP during the imaging of the ERTY transient, a decrease in the signal is observed in the

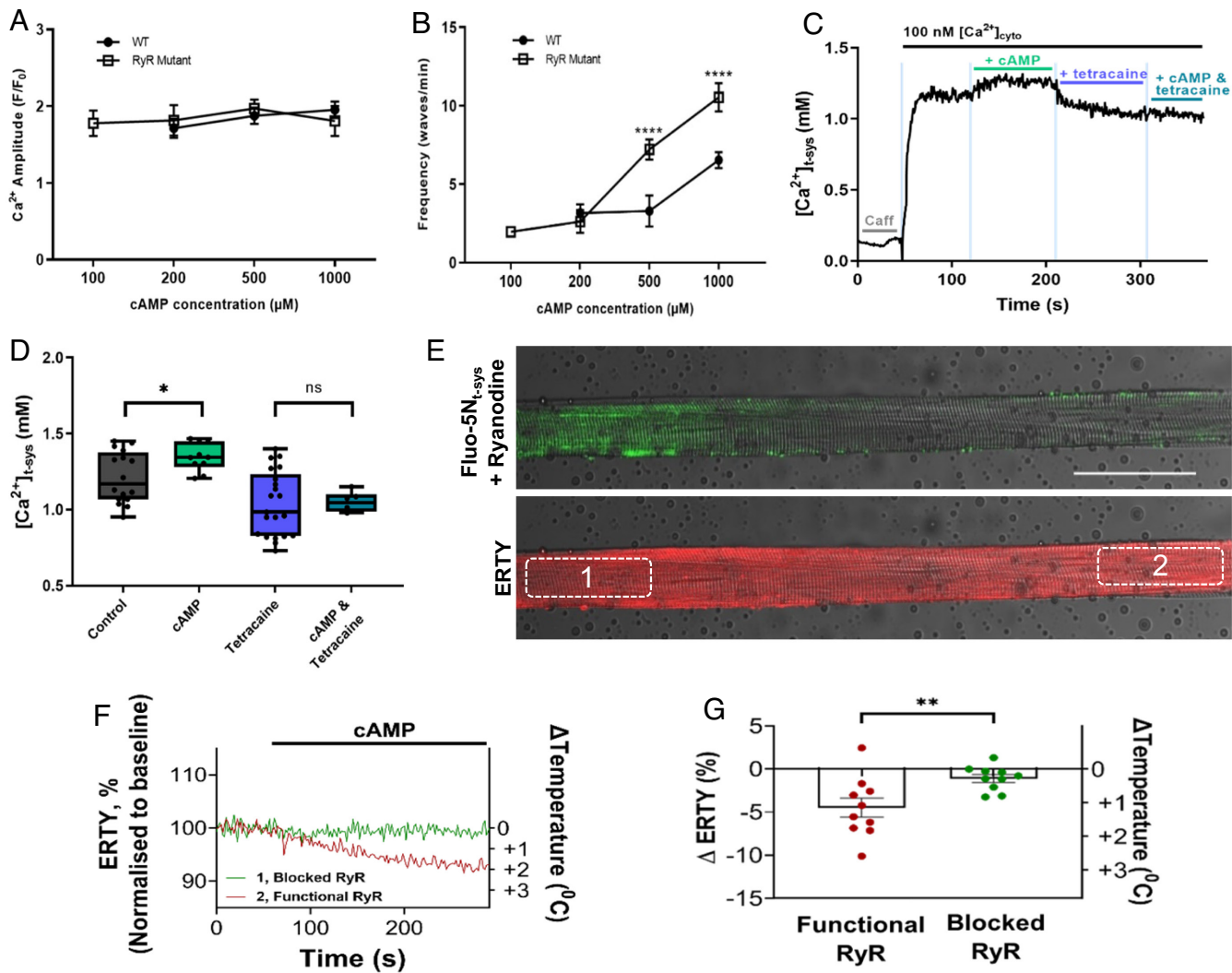


Fig. 4. cAMP induces Ca^{2+} release, increases RyR Ca^{2+} leak, and increases heat generation in mammalian skeletal muscle. *A*, normalized cytoplasmic rhod-2 fluorescence (F/F_0) of Ca^{2+} amplitudes between WT and RyR1 KI mice when exposed to varying concentrations of cAMP. *B*, wave frequency against [cAMP] summarized from *A*. *C*, the $[\text{Ca}^{2+}]_{\text{t-sys}}$ transient in WT mouse-skinned fiber, initially with SR thoroughly depleted by caffeine to chronically activate store-operated Ca^{2+} entry (2,35). The return to standard loading solution moved $[\text{Ca}^{2+}]_{\text{t-sys}}$ to mM levels. The addition of cAMP increased $[\text{Ca}^{2+}]_{\text{t-sys}}$ in the presence of a functional RyR. The subsequent addition of tetracaine to block the RyR lowered the $[\text{Ca}^{2+}]_{\text{t-sys}}$, indicating the increase in $[\text{Ca}^{2+}]_{\text{t-sys}}$ in the presence of cAMP was due to increased RyR Ca^{2+} leak. A combination of cAMP and tetracaine showed no difference to tetracaine alone, indicating that there were no off target effects of cAMP in this assay. *D*, summary $[\text{Ca}^{2+}]_{\text{t-sys}}$ in control ($n = 16$), cAMP ($n = 10$), tetracaine ($n = 21$), and tetracaine with cAMP ($n = 6$) (nested one-way ANOVA). *E*, representative confocal images of a mouse skeletal muscle fiber stained with ER thermo yellow, with and without the presence of fluo-5N and the RyR blocker ryanodine. *F*, ER thermo yellow fluorescence transients from same WT mouse fiber during the addition of 100 μM cAMP (functional RyR—red; blocked RyR—green). *G*, summary data of ER thermo yellow temperature change in the presence of a functional ($n = 10$) and blocked ($n = 10$) RyR, while exposed to cAMP. Data presented in *A*, *B*, and *G* as mean \pm SEM. Data presented in *D* as box and whisker plots (median, box indicates 25% and 75% percentile, whiskers indicate min and max data points). * $P < 0.05$, ** $P < 0.01$, **** $P < 0.0001$, ns = not significant. (Scale bar, 100 μm .)

section with functional RyR1s (red trace in Fig. 4*F* and region 2 in Fig. 4*E*) but not in the section with blocked RyR1s (green trace in Fig. 4*F* and region 1 in Fig. 4*E*). The decrease in ERTY signal indicates an increase in heat in the section with the functional RyR1s as cAMP is introduced, while there is no direct effect on the action of the SR Ca^{2+} pump, which does generate heat in isolation of RyR1 leak (1). A summary of results is shown in Fig. 4*G*. This result implicates the site of action of cAMP in mouse fast-twitch fibers to the RyR1. It is important to note that mouse fast-twitch fibers are void of sarcolipin and phospholamban that are sites of cAMP action and SR Ca^{2+} pump regulation (39).

The experiments presented in Fig. 4 indicate that brief exposure to cAMP has a functional effect on RyR1. We expect the functional change in RyR1 leak to be due to phosphorylation of the channel. To determine if this was the case, we underwent targeted

Western blotting to quantify the phosphorylation of RyR1 at Ser2844 (equivalent to Ser2843 in humans), which was found to be increased in cAMP (100 μM)-treated muscle compared with the matched control muscle (Fig. 5 *A* and *B*). Given there are multiple serine, threonine, and tyrosine potential phosphorylation sites on RyR1, we then undertook phosphoproteomics to identify other active sites. Within the threshold of detection, Ser2844 was the only site found to be phosphorylated (Fig. 5*C*).

Dantrolene Blocks Raising of RyR Ca^{2+} Leak. Dantrolene is a clinically approved muscle relaxant that targets the RyR (26). It has been used to provide indirect evidence that RyR Ca^{2+} leak is involved in the maintenance of core body temperature when mice were exposed to low ambient temperature stress (4 °C) (4). It was proposed that dantrolene inhibited RyR1-mediated Ca^{2+} leak in

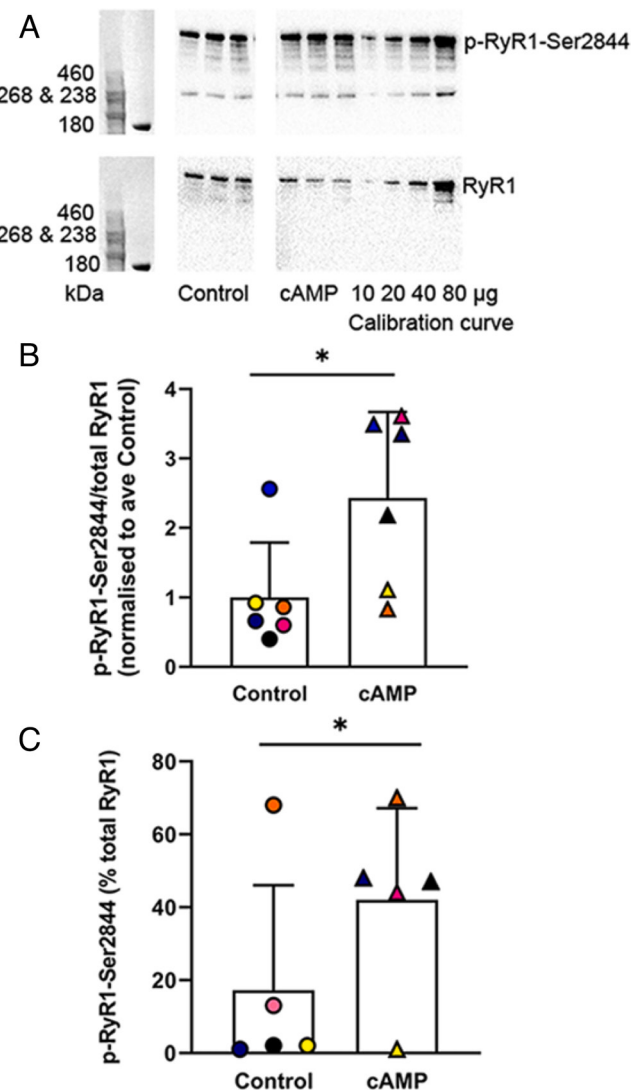


Fig. 5. Brief cAMP treatment phosphorylates RyR1 Ser2844. *A*, Western blot of EDL muscle from WT mice with or without exposure to 100 µM cAMP. The *Top* panel shows the probe using the human phospho-specific Ser 2843 RyR1 antibody (2844 in rodent muscle) and the *Bottom* shows total RyR1. Molecular weight markers on the *Left*, M1 high mark and M2 PageRuler, with indicative protein sizes shown on the left and in the lane. *B*, comparison of the amount of Ser2843/4 over total RyR1 in control and cAMP treated EDL samples detected by Western blotting, with each color denoting the same samples with different treatment ($P = 0.04$, $n = 6$ muscles). *C*, phosphoproteomics revealed that only the Ser2844 RyR1 site was detectable and this was significantly greater in treated compared with control samples ($P = 0.02$, $n = 5$ muscles, mean data of two treatments for M1, M2, and M4). * $P < 0.05$, 2-tailed, paired Student's *t* test. Symbols/animals: M1 (black), M2 (navy), M4 (pink), M6 (yellow), M8 (orange). Data presented in *B* and *C* as mean \pm SD.

these experiments, preventing the critical rise in $[Ca^{2+}]_{cyto}$ that is required to elevate SR Ca^{2+} pump activity for heat generation. It is known that dantrolene provides a partial block of the efflux of Ca^{2+} through the RyR, depending upon the prevailing cytoplasmic ionic conditions (40) and its effect on what might be considered a mild leak induced by intense *in vivo* contractions required the presence of 3 mM Mg^{2+} for dantrolene to provide a blockage of the leak (41). To provide direct evidence for the inhibition of RyR Ca^{2+} leak by dantrolene, mechanically skinned fiber experiments with t-system trapped rhod-5N like that in Fig. 4*D* were performed (2).

As shown in Fig. 6 *A* and *B*, the presence of 1 mM tetracaine at all four cytoplasmic Ca^{2+} concentrations significantly decreased the steady-state $[Ca^{2+}]_{t-sys}$ compared to the control, indicating a decrease in RyR1 leak as expected (2, 22). The presence of 10

µM dantrolene compared to the control was not significantly different at 28 nM and 67 nM $[Ca^{2+}]_{cyto}$, however was significantly lower at 200 nM and 1,342 nM $[Ca^{2+}]_{cyto}$. Both 200 nM and 1,342 nM $[Ca^{2+}]_{cyto}$ are above resting physiological levels, thus increasing $[Ca^{2+}]_{SR}$ (42), and inducing a higher level of RyR Ca^{2+} leak than typically expected in the resting fiber (2). At these cytoplasmic Ca^{2+} concentrations, dantrolene was effective at reducing RyR1 leak. Thus, we provide the mechanistic evidence for dantrolene blocking increased RyR1 Ca^{2+} leak, consistent with a requirement of mice maintenance of body temperature under low ambient temperature unless challenged with dantrolene in their circulation (4).

Discussion

Skeletal muscle of vertebrates use the same basic structures for EC coupling, where the SR releases Ca^{2+} to regulate contraction (43). The large volume of skeletal muscle in the body means that it can potentially provide a bed of warmth through the summation of the small amounts of heat constantly generated at the level of every sarcomere. This heat provides a means of insulating the body temperature against a cold environment. Mammals have achieved this in their resting muscles by evolving Ca^{2+} regulatory conditions that must show some departure from those in lower vertebrates that remain ectothermic, such as amphibians. To show the fundamental differences relevant to resting muscle regulating heat generation through the RyR, we applied an experimental approach of placing skinned fibers from toad and human MH-susceptible muscle perpendicular to each other, to create a common intersection between fibers, to observe how an abrupt rise in $[Ca^{2+}]$ is tolerated by each species. Our approach provides assessment of Ca^{2+} release mechanisms under identical ionic conditions that avoids cell damage induced by high-intensity laser light needed to uncage Ca^{2+} for abrupt local increases, as previously used by others to address similar questions (31). We show local, abrupt increase in $[Ca^{2+}]_{cyto}$ to a quiescent fiber caused loading of the SR with Ca^{2+} in mammalian muscle. This is key to providing a sustained leak of Ca^{2+} from the SR so the pump must work harder. This provides the capacity of mammalian muscle to operate as a heat generator.

The caveat on the endothermic strategy is the food consumption required to sustain basal heat generation compared to ectotherms. The ectothermic strategy is supported by a robust CICR mechanism (30). Our experiments showed that abrupt rises in $[Ca^{2+}]_{cyto}$ in toad quiescent fibers caused rapid Ca^{2+} release (Fig. 2). The activation of CICR puts a restriction on SR Ca^{2+} loading, to limit SR Ca^{2+} leak and therefore the ATP hydrolysis rate required to maintain the limited steady state $[Ca^{2+}]_{SR}$. Thus, the ectotherm reduces energy expenditure and the need to consume food compared to the endotherm, in part, due to the presence of the Ca^{2+} -sensitive RyR isoform in its muscle. In the heart, which is not required to act as a thermogenic organ, the presence of CICR and a substantially lower leak rate compared to RyR1, as in amphibian muscle (35), may indicate that a lower SR load is important to reduce energy expenditure.

In MH-susceptible and control human muscle fibers, even in the presence of the RyR agonist halothane, there was continued resistance to RyR1 activation by $[Ca^{2+}]_{cyto}$. The advantage of resistance to CICR activation is that a large range of local $[Ca^{2+}]_{cyto}$ at the RyR cytoplasmic face can be tolerated. Therefore, RyR1 Ca^{2+} leak rate can be adjusted to a required level to change ATP hydrolysis rate at the SR Ca^{2+} pump. This would make the system tuneable to required levels of heat generation via RyR-mediated leak (4).

The resistance of RyR1 to $[Ca^{2+}]_{cyto}$ also allowed RyR1 to become sensitive to other agonists (Figs. 1–3). Importantly for

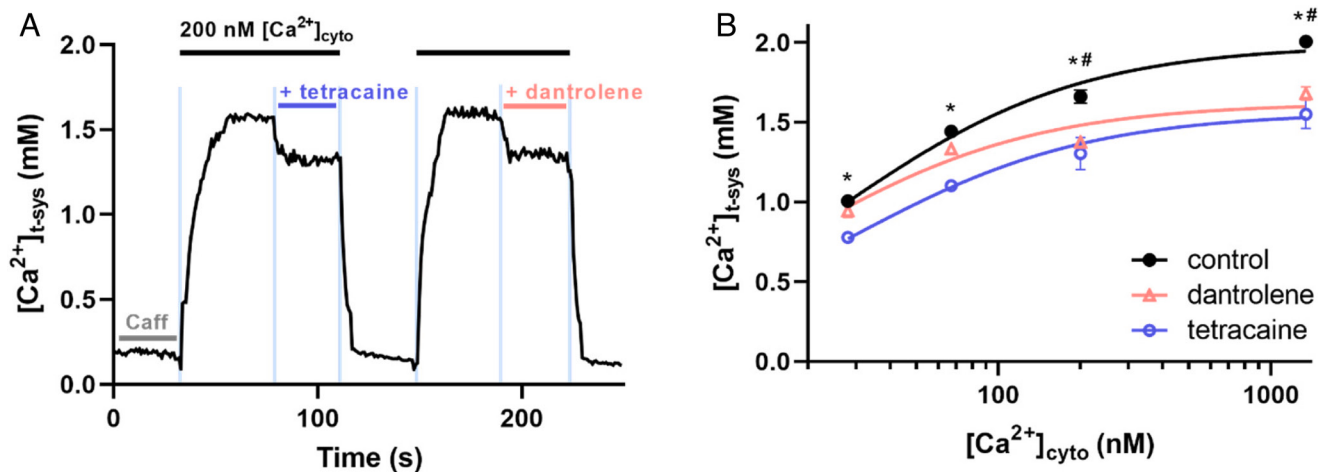


Fig. 6. Dantrolene blocks increased RyR Ca^{2+} leak. *A*, $[\text{Ca}^{2+}]_{\text{t-sys}}$ transient of a rat-skinned fiber exposed to the indicated solutions. *B*, summary of the effect of 10 μM dantrolene ($n = 6$ to 8 fibers per data point), full RyR Ca^{2+} leak block with 1 mM tetracaine ($n = 10$ to 12 fibers per data point) and no intervention (control) ($n = 18$ to 24 fibers per data point) on $[\text{Ca}^{2+}]_{\text{t-sys}}$ across a range of $[\text{Ca}^{2+}]_{\text{cyto}}$. T-tests of control vs. dantrolene (* $P < 0.05$); and control vs. tetracaine (** $P < 0.05$). Data presented as mean \pm SEM.

mammals, this means agonists, or second messengers released into the cytoplasm by the β -adrenergic system, like cAMP, can have an influence on the rate of Ca^{2+} leak from RyR1. That is, without $[\text{Ca}^{2+}]_{\text{cyto}}$ opening the RyR to release Ca^{2+} , there can be increased sensitivity to cAMP to increase RyR Ca^{2+} leak. The acute response of the SNS to activate mammalian skeletal muscle RyR leak as ambient temperature is lowered was indirectly shown by Bal et al. (2012) by interrupting muscle-based thermogenesis with circulating dantrolene (4). By using a fiber-based assay, we confirm that the dantrolene blocks only high rates of RyR Ca^{2+} leak in mouse skeletal muscle (Fig. 6), consistent with RyR1 Ca^{2+} leak being raised in the mice exposed to 4 °C (4). Linking these two results provides evidence for this hypothesis but is still not direct evidence that cold-sensing at the skin leads to increased RyR leak. It is not currently possible to make such fine measurements of RyR Ca^{2+} leak or SR temperature at the muscle in a live mouse with an intact SNS.

We have recently shown that the SR Ca^{2+} pump of mouse fast-twitch fibers underlies the generation of significant heat at rest, and this is further amplified by RyR1 Ca^{2+} leak (1). We can now extend the description of mammalian thermogenesis to involve the phosphorylation of RyR1 at Ser2843/4 in the presence of cAMP. Together, these results show that the β -adrenergic system works to rapidly increase RyR1 Ca^{2+} leak in the muscle to resist changes in body temperature in cold environments. Furthermore, our demonstration that heat generation can be modulated in muscle fibers void of sarcolipin (1, 39) (Figs. 4 and 5) indicates that this protein is not primarily necessary for thermogenesis.

Basal Ca^{2+} leak through RyR1 is important for multiple functions in skeletal muscle, including triggering adaptation to exercise (44, 45), coupling with SOCE to redistribute fiber Ca^{2+} among the SR, cytoplasm, and mitochondria, which, for example, assists with adjusting Ca^{2+} release quanta for EC coupling (22, 36, 46). It is not clear whether thermogenesis was a primary driver for the isolation of the RyR1 in mammalian skeletal muscle, or whether thermogenesis was a subsequent adaptation to or parallel driver for RyR1 isolation for leak to act as a signal for muscle adaptation or other functional advantages. Further studies comparing the influence of RyR Ca^{2+} leak on physiological responses in ectothermic vertebrate skeletal muscle with that of mammals may provide some clarity around this issue.

Here we have shown resistance of RyR1 to CICR in the face of rising $[\text{Ca}^{2+}]_{\text{cyto}}$ in mammalian skeletal muscle is key to providing a large range of $[\text{Ca}^{2+}]_{\text{cyto}}$ to the pump for heat generation in relaxed muscle, including in human muscle with a gain-of-function *RYR1* mutation. This outcome provides a platform for stable heat generation regulated by the β -adrenergic system so that RyR Ca^{2+} leak can be regulated by [agonist], most likely through cAMP release and subsequent RyR1 phosphorylation. CICR is a relatively slow mechanism, unsuitable for EC coupling in skeletal muscle that is likely in place in amphibians to limit SR Ca^{2+} load and Ca^{2+} leak (23, 29), to conserve energy. By relieving the mammalian muscle of a Ca^{2+} -sensitive RyR isoform, a futile cycle of Ca^{2+} through the SR can be amplified, providing heat for mammals even while they are lying still. This was a major evolutionary benefit that allowed mammals to spread to all parts of the globe.

Methods

Muscle Preparation. All experiments were approved by the University of Queensland Human and Animal Ethics Committee or the La Trobe University Animal Ethics Committee and were performed in accordance with the relevant guidelines and regulations. Human subjects provided informed consent before proceeding with muscle biopsies. Subjects were previously diagnosed as malignant hyperthermia-susceptible or non-susceptible via genetic testing and/or an in-vitro contracture test (47). Human muscle biopsies were collected under local anesthesia (xylocaine, 10 mg mL⁻¹) from the mid-portion of the vastus lateralis muscle, using a 6-mm Bergstrom biopsy needle modified for manual suction (48). Muscle tissue collected from the biopsy needle was blotted on filter paper to remove blood and external fluid. Muscle tissue was pinned to Sylgard set in a petri dish containing paraffin oil.

Male Wistar rats (6 to 8 weeks old), male (3 to 5 mo old) C57BL/6J and *RYR1* KI [p.G2435R variant (25)] mice were euthanized by asphyxiation via CO₂ exposure, and the extensor digitorum longus (EDL) was rapidly excised (20). Cane toads (*R. marina*) were euthanized by double pithing and the iliofibularis (IL) muscle was rapidly excised. Once dissected, muscles were pinned to Sylgard set in a petri dish containing paraffin oil.

Skinned fibers were used for confocal Ca^{2+} imaging experiments (26). Briefly, fine-tipped jeweller's forceps were used to isolate a single muscle fiber from the muscle belly under a dissecting microscope. The single fiber is then mechanically skinned by peeling the sarcolemma back along the length of the fiber forming a visible cuff. The fiber is then transferred to a custom-built chamber which allows the direct manipulation of the intracellular environment by bathing the preparation in solutions of differing ionic composition.

Tracking Cytoplasmic Regenerative Ca^{2+} Waves. Skinned fibers were prepared and bathed in a resting physiological solution containing 100 nM Ca^{2+} , 1 mM Mg^{2+} , 36 mM Na^+ , 126 mM K^+ , 100 μM EGTA, 90 mM HEPES, 5 mM rhod-2, 10 mM creatine phosphate, and 8 mM ATP. The pH was adjusted to 7.1 with KOH. The Ca^{2+} -sensitive dye rhod-2 was used to track Ca^{2+} transients, and the contractile apparatus inhibitor n-benzyl-p-toluene sulfonamide (BTS) was added to prevent fiber movement. Ca^{2+} waves were generated by substituting the resting solution for a solution of the same composition with the addition of RyR agonists halothane (1 mM) or caffeine (3 mM). Fluorescence signals were imaged in xyt mode on a Zeiss LSM 5 live under a 0.45NA 10x Plan-Apochromat objective. To obtain Ca^{2+} amplitude fluorescence, a region of interest was selected within the boundary of a fiber and then the average fluorescence was normalized to baseline recordings, presented as F/F_0 . Wave frequency was calculated as the number of waves passing through the fiber over time and presented as waves per minute.

Abrupt, Local Elevation of $[\text{Ca}^{2+}]$ in Skinned Fiber Preparation. To stimulate a local increase in $[\text{Ca}^{2+}]_{\text{cyto}}$ two mechanically skinned fibers were positioned perpendicularly to each other, in a "cross" formation, so both fibers had a common intersection. The rationale was that a Ca^{2+} wave passing on an activated fiber would provide an abrupt, local rise in $[\text{Ca}^{2+}]_{\text{cyto}}$ in the quiescent fiber. The design made it possible to examine the response of fibers from different species to the abrupt increase in local $[\text{Ca}^{2+}]_{\text{cyto}}$. The crossing of different fibers provides a means to assess the response of different RyR isoforms and different inherent RyR Ca^{2+} leak rates in resting fibers to abruptly increasing cytoplasmic $[\text{Ca}^{2+}]$ under identical ionic conditions. The following combinations were performed: toad fiber vs. toad fiber; human MHS vs. human MHS; toad fiber vs. human MHS; and toad fiber vs. human MHN.

The amount of time required for a Ca^{2+} wave to propagate at the intersection with the quiescent fiber was calculated using Image J software and expressed as "delay in Ca^{2+} release at quiescent fiber junction." Briefly, a region of interest was located on the quiescent fiber near the junction and a >100% increase in baseline fluorescence indicated wave propagation. The time was initiated when a wave from the active fiber reached the junction (shown in Fig. 1A, panel labelled 1 s) then ceased when the above-mentioned propagation occurred. In some experiments, a Leica DMi8 SP8 confocal microscope with a Leica 20 \times objective with a temperature-controlled incubation chamber that encompassed the stage was used. The incubation chamber was set to a temperature of $32 \pm 1^\circ\text{C}$. Fibers were allowed ~ 10 min equilibration in the incubation chamber prior to imaging.

In some Ca^{2+} wave experiments, skinned fibers were bathed in a standard solution with 10 μM fluo-5NAM, 10 μM carbonilcyanide *p*-trifluoromethoxyphenylhydrazone (FCCP), and 0.05% Pluronic F-127 detergent to load fluo-5N into the SR to allow tracking of $[\text{Ca}^{2+}]_{\text{SR}}$. The fibers were then incubated at 37 °C for 30 min. Fibers loaded in this manner were used in single fiber and cross fiber experiments.

Detecting RyR Ca^{2+} Leak in Skeletal Muscle. Bundles of fibers were isolated and exposed to an internal solution containing 145 mM NaCl , 3 mM KCl, 2.5 mM CaCl_2 , 2 mM MgCl_2 , 2.5 mM rhod-5N salt, 0.05 mM BTS, and 10 mM HEPES (pH 7.1). Bundles were allowed 15 min to equilibrate with the physiological solution and then individual fibers were isolated and mechanically skinned. Skinned fibers with fluorescent dye trapped in the t-system were mounted on a custom-made chamber and bathed in a standard loading solution: 50 mM EGTA, 90 mM HEPES, 126 mM K^+ , 36 mM Na^+ , 8 mM ATP, 1 mM Mg^{2+} , 10 mM creatine phosphate, and 100 nM Ca^{2+} . For each experimental trial, Ca^{2+} was loaded into the SR and t-system in a standard loading solution with a range of 28 to 1,342 nM Ca^{2+} while being continuously imaged. SR and t-system Ca^{2+} was released with 30 mM caffeine in an internal solution with 0.01 mM Mg^{2+} .

Mounted skinned fibers were imaged using an Olympus FV1000 confocal microscope with an 0.9NA 40 \times Plan-Apochromat objective. Rhod-5N was excited with 543 nm HeNe laser, and the emission was filtered using the Olympus spectra detector. For tracking Ca^{2+} movements across the t-system membrane, images were continuously recorded in xyt mode with an aspect ratio of 256 \times 512, with the long aspect of the image parallel with that of the preparation. Each frame was captured in 0.8 s.

T-system rhod-5N fluorescence was converted to $[\text{Ca}^{2+}]_{\text{t-sys}}$ as previously described (49):

$$[\text{Ca}^{2+}]_{\text{t-sys}}(t) = K_d \frac{(F(t) - F_{\min})}{(F_{\max} - F(t))}.$$

The K_d of rhod-5N was 0.872 mM (35). F_{\max} was determined by applying a physiological solution with ionomycin and 5 mM Ca^{2+} . F_{\min} was determined by applying a solution with 50 mM EGTA and no added Ca^{2+} .

Isolated mechanically skinned fibers were continuously imaged as described above, to obtain a record of t-system rhod-5N fluorescence changes over time as the cytoplasmic solution bathing the fiber was changed. SR and t-system Ca^{2+} was released by bathing the fiber in a solution where free $[\text{Mg}^{2+}]$ was lowered from 1 to 0.01 mM in the presence of 30 mM caffeine (release solution). This chronically opened the RyR, thus thoroughly depleting the SR of Ca^{2+} and consequent depletion of t-system Ca^{2+} occurred via the activation of SOCE. Alternatively, the application of 200 nM $[\text{Ca}^{2+}]_{\text{cyto}}$ standard internal solution allowed the uptake of Ca^{2+} and the $[\text{Ca}^{2+}]_{\text{t-sys}}$ reached a steady-state that was partially dependent on Ca^{2+} leaking through RyRs into the tight junctional space between the t-system and SR membranes (2). Furthermore, free $[\text{Ca}^{2+}]$ in the standard internal solution can be varied in the range of 28 nM to 1.3 μM , which alters Ca^{2+} leak from the RyR. By blocking the RyR with tetracaine (1 mM), it was possible to separate the influence of RyR Ca^{2+} leak on t-system Ca^{2+} steady state from the level determined by the lower concentration of bulk cytoplasmic Ca^{2+} that could otherwise enter the junctional space. This difference provides a measure of RyR Ca^{2+} leak, or a reference for Ca^{2+} leak that we can use to assess RyR agonists (cAMP) or inhibitors (dantrolene).

cAMP Effect on RyR Ca^{2+} Release and Ca^{2+} Leak. Mechanically skinned fibers were prepared from the EDL muscles of male C57BL/6J mice (presented as wild type, WT) and from heterozygous male *RYR1* KI mice. Regenerative Ca^{2+} waves were induced within both WT and MHS-mutant groups with cAMP (3',5'-Cyclic AMP sodium salt, Sigma-Aldrich). cAMP was dissolved as a stock solution in H_2O and added to physiological solution at 100 μM , 200 μM , 500 μM , and 1,000 μM .

Ca^{2+} leak in the WT group was examined using the t-system rhod-5N Ca^{2+} leak assay. To determine the downstream effects of beta-adrenergic stimulation, cAMP was applied and RyR Ca^{2+} leak was assessed. cAMP was dissolved as a stock solution in H_2O and added to internal solution at 100 μM . Tetracaine was dissolved as a stock solution in DMSO and applied at a concentration of 1 mM.

ER Thermo Yellow Staining. Skeletal muscle fibers from WT mice were prepared as described (1). Briefly, a discrete section of isolated fibers were exposed to fluo-5N (1 mM) and RyR blocker ryanodine (50 μM). Fibers were then mechanically skinned and placed in a physiological solution containing 500 nM ERTY and incubated for 30 min at 37 °C. The solution was then replaced with a standard solution with 100 nM Ca^{2+} (no ERTY) and imaged on an Olympus FV1000 confocal microscope. ERTY fluorescence signal and temperature have been calibrated previously, with the signal changing at 3.9% per 1 °C (50).

Whole Muscle Preparation and cAMP Treatment for Biochemical Analysis. Whole tissue homogenate samples were prepared by homogenizing ~5 mg of frozen EDL muscle (1:50 wt/vol) using a handheld polytron homogenizer (Polytron PT 1200E Kinematica, Lucerne, Switzerland) three times at maximum speed for 5 to 10 s in the ice-cold homogenizing solution (50 mM HDTA, 90 mM HEPES, 126 mM K^+ , 36 mM Na^+ , 8 mM ATP, 8.5 mM total Mg^{2+} , 10 mM creatine phosphate (pH 7.10) with phosphatase inhibitor (PhosSTOP; Roche Diagnostics, Mannheim, Germany), 295 ± 10 mosmol/kg H_2O). Following homogenization, whole muscle samples were vortexed three times at maximum speed for ~10 s and then diluted to 10 $\mu\text{g}/\mu\text{L}$ in homogenizing solution. The homogenate samples were then divided into three tubes (50 to 100 μL each) for control and cAMP-treatments (cAMP). We performed treatments using sodium-salt cAMP (Sigma A6885, same as fiber Ca^{2+} experiments). For cAMP treatment, cAMP was added to the whole muscle homogenates at 100 μM , using a stock solution (dissolved in ddH₂O). Samples were vortexed for ~10 s then left for 1 min at room temperature (~23 °C). After 1 min, 3XSDS loading buffer was added (2:1 v/v) to all samples, which were then incubated at RT for ~1 h and stored at -80 °C until Western blot analysis.

Western Blotting. Samples (50 µg) were separated on 4 to 12% Criterion XT Bis-Tris gels (Bio-Rad Laboratories) at 200 V for 1 h and transferred to nitrocellulose membranes via wet transfer at 100 V for 30 min. A calibration curve, constructed from a mixture of all experimental samples was also loaded along with protein markers (High-Mark, Invitrogen and PageRuler Prestained, Thermo Fisher Scientific). After transfer, the gel was stained with Coomassie G-250 (Bio-Rad Laboratories) for 1 h and destained overnight in ddH₂O. The membrane was rocked in Miser antibody extender for 10 min, washed in ddH₂O, and then blocked buffer [5% skim milk in 1× tris-buffered saline with Tween 20 (1×TBST)] for 90 min at RT. The membrane was then incubated with primary antibodies for 2 h at RT and overnight at 4 °C. The phospho-specific RyR1 antibody (1:5,000 dilution, rabbit polyclonal, Affinity Biosciences, AF3703) targeted to the phosphorylation of serine 2843 of the human RyR1 sequence was applied (which corresponds to Ser2844 in mouse RyR1). Following overnight incubation, the membrane was washed in blocking buffer and incubated with rabbit (1:20,000, 31,460, Thermo Fisher Scientific) secondary antibody for 1 h at RT followed by three washes in 1×TBST. The protein bands were visualized after applying SuperSignal West Femto chemiluminescent substrate (Thermo Fisher Scientific). Molecular weight markers were exposed under white light, chemiluminescent images were captured without moving the membrane using Chemidoc MP System, and densitometry was performed using Image Lab 5.2.1 (Bio-Rad). After imaging pRyR1-Ser2843, the membrane was washed in 1×TBST and then incubated with a total RyR1 antibody (1:200, mouse, DSHB, 34C) without stripping the membrane and the same steps were repeated but with the mouse-specific secondary antibody (1:20,000, 31,430, Thermo Fisher Scientific).

The p-RyR1-Ser2844 and total RyR1 signals for each sample were normalized to their respective calibration curves on the same gel before calculating the ratio of phosphorylated RyR1/total RyR1, which was then expressed relative to the average of the Control samples.

Phosphoproteomics. Control and cAMP-treated samples ($n = 5$) were run on Bis-Tris gel (as described for Western blotting) and after destaining, the gel was from ~270 kDa to the top of the gel. The excised gel pieces were frozen at -80 °C until mass spectrometry analysis.

The excised gel pieces were treated with 100 µL of acetonitrile and left at room temperature for 15 min, after which the acetonitrile was removed to waste. The samples were then reduced with 100 µL of 10 mM dithiothreitol (DTT) dissolved in 100 mM ammonium bicarbonate for 30 min at 37 °C. The DTT solution was then discarded. Next, the samples were alkylated by adding 100 µL of 50 mM iodoacetamide dissolved in 100 mM ammonium bicarbonate for 30 min at 37 °C (the samples were protected from light during the alkylation reaction). The alkylation solution was then removed to waste and the gel pieces were washed twice with 100 mM ammonium bicarbonate/10% acetonitrile (v/v). The gel pieces were then dehydrated by adding 100 µL of acetonitrile for 15 min, after which the acetonitrile was discarded, and the gel pieces were left to air dry for 10 min. The protein in the dehydrated gel pieces was digested by adding 40 µL of sequencing-grade trypsin (15 ng/µL) and incubated for 45 min on ice until the gel pieces

were rehydrated. An additional 40 µL of 25 mM ammonium bicarbonate was added, followed by incubation at 37 °C for 16 h. The peptides were extracted from the gel pieces by adding 60 µL of a 0.1% formic acid/60% acetonitrile solution (v/v) for 30 min at room temperature. The gel pieces were pelleted by centrifugation, and the peptides in the supernatant were removed to fresh tubes. The peptide samples were acidified by adding formic acid to a final concentration of 1% and then lyophilized. Prior to mass spectrometry analysis, the samples were reconstituted in 12 µL of 0.1% formic acid/2% acetonitrile (v/v). The tryptic peptides were analyzed by LC-MS/MS using a TimsTOF Pro mass spectrometer fitted with a Thermo Ultimate 3,000 HPLC.

Label-free quantification intensities were used for comparison between samples that were run in parallel. For proteins with an intensity value of 0, the minimum (background) intensity value measured from a given run was used to perform the ratio calculations. This value represents the minimum intensity measured for all identified proteins. The data are presented as a percentage of the total RyR1 intensity (i.e., phosphorylation and dephosphorylation intensities).

Statistical Analysis. GraphPad prism was used to perform all statistical analysis. To determine statistical difference, a Student's unpaired *t* test, one-way ANOVA with Tukey's post hoc test or two-way ANOVA with Tukey's post hoc test was performed. A nested *t* test and nested one-way ANOVA was performed where appropriate to identify potential variation between fibers and organisms. Significance was accepted at $P < 0.05$.

Biochemical and proteomic data were tested for assumptions of normality using a Shapiro-Wilk test. Phosphoproteomic data (control samples) were transformed ($y = 1/y$) prior to statistical analysis. For visual clarity, non-transformed data are presented in all figures. A Student's paired *t* test was used to compare the levels of pRyR1-Ser2844 between control and cAMP-treated samples from Western blotting and phosphoproteomic analyses.

Data, Materials, and Software Availability. All study data are included in the article and/or *SI Appendix*.

ACKNOWLEDGMENTS. We thank the editor and staff at PNAS for allowing an extended revision period for this work in light of unavoidable delays due to the ill-health of one of the authors. We thank Jeff Coombes (University of Queensland) for muscle biopsies; and Philip Hopkins and Paul Allen (University of Leeds) for providing the *RYR1* KI mice. This work was supported by an Australian Research Council Discovery Project (DP220102018) to B.S.L. and R.M.M.

Author affiliations: ^aSchool of Biomedical Sciences, The University of Queensland, Brisbane, QLD 4072, Australia; ^bDepartment of Biochemistry and Chemistry, La Trobe Institute for Molecular Science, School of Agriculture, Biomedicine and Environment, La Trobe University, Melbourne, VIC 3083, Australia; ^cDrug Discovery Biology Unit, Monash Institute of Pharmaceutical Sciences, Monash University, Melbourne, VIC 3052, Australia; and ^dThe Florey Institute of Neuroscience and Mental Health, Melbourne, VIC 3052, Australia

1. A. Meizoso-Huesca, L. Pearce, C. J. Barclay, B. S. Launikonis, Ca²⁺ leak through ryanodine receptor 1 regulates thermogenesis in resting skeletal muscle. *Proc. Natl. Acad. Sci. U.S.A.* **119**, e2119203119 (2022).
2. T. R. Cully et al., Junctional membrane Ca²⁺-dynamics in human muscle fibers are altered by malignant hyperthermia causative RyR mutation. *Proc. Natl. Acad. Sci. U.S.A.* **115**, 8215–8220 (2018).
3. B. A. Block, Thermogenesis in muscle. *Annu. Rev. Physiol.* **56**, 535–577 (1994).
4. N. C. Bal et al., Sarcolipin is a newly identified regulator of muscle-based thermogenesis in mammals. *Nat. Med.* **18**, 1575–1579 (2012).
5. J. P. Costanzo, R. E. Lee Jr., A. L. DeVries, T. Wang, J. R. Layne Jr., Survival mechanisms of vertebrate ectotherms at subfreezing temperatures: Applications in cryomedicine. *FASEB J.* **5**, 351–358 (1995).
6. K. B. Storey, J. M. Storey, Molecular physiology of freeze tolerance in vertebrates. *Physiol. Rev.* **97**, 623–665 (2017).
7. T. Murayama, Y. Ogawa, Selectively suppressed Ca²⁺-induced Ca²⁺ release activity of alpha-ryanodine receptor (alpha-RyR) in frog skeletal muscle sarcoplasmic reticulum: Potential distinct modes in Ca²⁺ release between alpha- and beta-RyR. *J. Biol. Chem.* **276**, 2953–2960 (2001).
8. W. Melzer, A. Herrmann-Frank, H. C. Luttgau, The role of Ca²⁺ ions in excitation-contraction coupling of skeletal muscle fibres. *Biochim. Biophys. Acta* **1241**, 59–116 (1995).
9. G. D. Lamb, Excitation-contraction coupling in skeletal muscle: Comparisons with cardiac muscle. *Clin. Exp. Pharmacol. Physiol.* **27**, 216–224 (2000).
10. E. Rios, Calcium-induced release of calcium in muscle: 50 years of work and the emerging consensus. *J. Gen. Physiol.* **150**, 521–537 (2018).
11. M. Endo, Calcium-induced calcium release in skeletal muscle. *Physiol. Rev.* **89**, 1153–1176 (2009).
12. V. Lukyanenko, J. M. Muriel, R. J. Bloch, Coupling of excitation to Ca²⁺ release is modulated by dysferlin. *J. Physiol.* **595**, 5191–5207 (2017).
13. R. Takagi, A. Tabuchi, D. Poole, Y. Kano, In vivo cooling-induced intracellular Ca²⁺ elevation and tension in rat skeletal muscle. *Physiol. Rep.* **9**, 13 (2021).
14. N. Shirokova, J. García, G. Pizarro, E. Ríos, Ca²⁺ release from the sarcoplasmic reticulum compared in amphibian and mammalian skeletal muscle. *J. Gen. Physiol.* **107**, 1–18 (1996).
15. N. Shirokova, J. García, E. Ríos, Local calcium release in mammalian skeletal muscle. *J. Physiol.* **512**, 377–84 (1998).
16. N. Shirokova et al., Spatially segregated control of Ca²⁺ release in developing skeletal muscle of mice. *J. Physiol.* **521**, 483–495 (1999).
17. B. S. Launikonis, D. G. Stephenson, Effects of Mg²⁺ on Ca²⁺ release from sarcoplasmic reticulum of skeletal muscle fibres from yabby (crustacean) and rat. *J. Physiol.* **526**, 299–312 (2000).
18. T. R. Cully, J. N. Edwards, B. S. Launikonis, Activation and propagation of Ca²⁺ release from inside the sarcoplasmic reticulum network of mammalian skeletal muscle. *J. Physiol.* **592**, 3727–3746 (2014).
19. M. G. Klein, L. Kovacs, B. J. Simon, M. F. Schneider, Decline of myoplasmic Ca²⁺, recovery of calcium release and sarcoplasmic Ca²⁺ pump properties in frog skeletal muscle. *J. Physiol.* **441**, 639–671 (1991).
20. M. W. Fryer, D. G. Stephenson, Total and sarcoplasmic reticulum calcium contents of skinned fibres from rat skeletal muscle. *J. Physiol.* **493**, 357–370 (1996).
21. C. J. Barclay, B. S. Launikonis, Components of activation heat in skeletal muscle. *J. Muscle. Res. Cell. Motil.* **42**, 1–16 (2019).
22. C. R. Lambole et al., Ryanodine receptor leak triggers fibre Ca²⁺ redistribution to preserve force and elevate basal metabolism in skeletal muscle. *Sci. Adv.* **7**, eabi7144 (2021).

23. B. S. Launikonis *et al.*, Confocal imaging of [Ca²⁺] in cellular organelles by SEER, shifted excitation and emission ratioing of fluorescence. *J. Physiol.* **567**, 523–543 (2005).
24. D. M. Bers, Cardiac excitation-contraction coupling. *Nature* **415**, 198–205 (2002).
25. J. R. Lopez, V. Kaura, C. P. Diggle, P. M. Hopkins, P. D. Allen, Malignant hyperthermia, environmental heat stress, and intracellular calcium dysregulation in a mouse model expressing the p. G2435R variant of RYR1. *Br. J. Anaesth.* **121**, 953–961 (2018).
26. G. D. Lamb, D. G. Stephenson, Measurement of force and calcium release using mechanically skinned fibres from mammalian skeletal muscle. *J. Appl. Physiol.* **125**, 1105–1127 (2018).
27. N. Shirokova, E. Ríos, Small event Ca²⁺ release: A probable precursor of Ca²⁺ sparks in frog skeletal muscle. *J. Physiol.* **502**, 3–11 (1997).
28. T. Murayama, N. Kurebayashi, Y. Ogawa, Role of Mg²⁺ in Ca²⁺-induced Ca²⁺ release through ryanodine receptors of frog skeletal muscle: Modulations by adenine nucleotides and caffeine. *Biophys. J.* **78**, 1810–1824 (2000).
29. T. Murayama, N. Kurebayashi, Two ryanodine receptor isoforms in nonmammalian vertebrate skeletal muscle: Possible roles in excitation-contraction coupling and other processes. *Prog. Biophys. Mol. Biol.* **105**, 134–144 (2011).
30. M. Endo, M. Tanaka, Y. Ogawa, Calcium induced release of calcium from the sarcoplasmic reticulum of skinned skeletal muscle fibres. *Nature* **228**, 34–36 (1970).
31. L. Figueroa *et al.*, Synthetic localized calcium transients directly probe signalling mechanisms in skeletal muscle. *J. Physiol.* **590**, 1389–1411 (2012).
32. L. Landsberg, M. E. Saville, J. B. Young, Sympathoadrenal system and regulation of thermogenesis. *Am. J. Physiol.* **247**, E181–E189 (1984).
33. G. S. Lynch, J. G. Ryall, Role of beta-adrenoceptor signaling in skeletal muscle: Implications for muscle wasting and disease. *Physiol. Rev.* **88**, 729–767 (2008).
34. S. P. Cairns, F. Borroni, β -Adrenergic modulation of skeletal muscle contraction: Key role of excitation-contraction coupling. *J. Physiol.* **593**, 4713–4727 (2015).
35. J. W. Bassani, W. Yuan, D. M. Bers, Fractional SR Ca release is regulated by trigger Ca and SR Ca content in cardiac myocytes. *Am. J. Physiol.* **268**, 1313–1319 (1995).
36. L. Pearce *et al.*, Ryanodine receptor activity and store-operated Ca²⁺ entry: Critical regulators of Ca²⁺ content and function in skeletal muscle. *J. Physiol.*, 10.1111/jp279512 (2022).
37. W. A. Macdonald, D. G. Stephenson, Effects of ADP on sarcoplasmic reticulum function in mechanically skinned skeletal muscle fibres of the rat. *J. Physiol.* **532**, 499–508 (2001).
38. C. J. Barclay, B. S. Launikonis, A mathematical model to quantify RYR Ca²⁺ leak and associated heat production in resting human skeletal muscle fibers. *J. Gen. Physiol.* **154**, e202112994 (2022).
39. N. C. Bal *et al.*, Is upregulation of sarcolipin beneficial or detrimental to muscle function? *Front. Physiol.* **12**, 633058 (2021).
40. R. H. Choi, X. Koenig, B. S. Launikonis, Dantrolene requires Mg²⁺ to arrest malignant hyperthermia. *Proc. Natl. Acad. Sci. U.S.A.* **114**, 4811–4815 (2017).
41. D. Watanabe, M. Wada, Orthograde signal of dihydropyridine receptor increases Ca²⁺ leakage after repeated contractions in rat fast-twitch muscle in vivo. *AJP Cell Physiol.* **320**, 806–821 (2021).
42. X. Koenig *et al.*, Mechanistic insights into store-operated Ca²⁺ entry during excitation-contraction coupling in skeletal muscle. *Biochim. Biophys. Acta Mol. Cell Res.* **1866**, 1239–1248 (2019).
43. C. Franzini-Armstrong, The relationship between form and function throughout the history of excitation-contraction coupling. *J. Gen. Physiol.* **150**, 189–210 (2018).
44. N. Ivarsson *et al.*, SR Ca²⁺ leak in skeletal muscle fibers acts as an intracellular signal to increase fatigue resistance. *J. Gen. Physiol.* **151**, 567–577 (2019).
45. C. Seng *et al.*, Tiny changes in cytoplasmic [Ca²⁺] cause large changes in mitochondrial Ca²⁺: What are the triggers and functional implications? *AJP Cell Physiol.* **323**, 1285–1289 (2022).
46. R. L. Gillies, A. R. Bjorksten, D. Du Sart, B. M. Hockey, Analysis of the entire ryanodine receptor type 1 and alpha 1 subunit of the dihydropyridine receptor (CACNA1S) coding regions for variants associated with malignant hyperthermia in Australian families. *Anaesth. Intensive Care* **43**, 157–166 (2015).
47. T. R. Cully *et al.*, Human skeletal muscle plasmalemma alters its structure to change its Ca²⁺-handling following heavy-load resistance exercise. *Nat. Commun.* **8**, 14266 (2017).
48. T. R. Cully, J. N. Edwards, R. M. Murphy, B. S. Launikonis, A quantitative description of tubular system Ca²⁺-handling properties in fast- and slow-twitch fibres. *J. Physiol.* **594**, 2795–2810 (2016).
49. S. Arai, S. Lee, D. Zhai, M. Suzuki, Y.T. Chang, A molecular fluorescent probe for the targeted visualization of temperature at the endoplasmic reticulum. *Sci. Rep.* **4**, 6701 (2014).
50. R. M. Murphy, N. T. Larkins, J. P. Mollica, N. A. Beard, G. D. Lamb, Calsequestrin content and SERCA determine normal and maximal Ca²⁺ storage levels in sarcoplasmic reticulum of fast- and slow-twitch fibres of rat. *J. Physiol.* **587**, 443–460 (2009).